International Journal of Disaster Risk Reduction 115 (2024) 105023

Contents lists available at ScienceDirect

International Journal of Disaster Risk Reduction

journal homepage: www.elsevier.com/locate/ijdrr

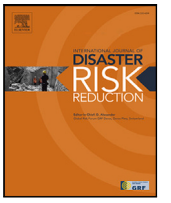

Reinforcement learning-based tsunami evacuation guidance system

Erick Mas [a], Luis Moya [b,*], Edgard Gonzales [c], Shunichi Koshimura [a]

[a] International Research Institute of Disaster Science, Tohoku University, Aoba 468-1 E401, Aramaki, Aoba-ku, Sendai, 980-8572, Miyagi, Japan

[b] GERDIS research group, Department of Engineering, Pontificia Universidad Católica del Perú, Av. Universitaria 1801, San Miguel, Lima, 15088, Peru

[c] Faculty of Geology, Geophysics and Mines, Universidad Nacional de San Agustín de Arequipa, Santa Catalina Nro. 117, Arequipa, Peru

ARTICLE INFO

Keywords:
Agent-based model
Tsunami evacuation
Reinforcement learning
Evacuation simulation

ABSTRACT

Congestion and crowding are critical issues during indoor and outdoor emergency evacuations. In the 2011 Great East Japan Earthquake and Tsunami, vehicle traffic was one of the causes of the event's casualties. After this, vehicle evacuation in tsunami events is not advised in Japan. Then, pedestrian evacuation is expected to be the primary mode of mobility in emergencies. However, crowding and congestion may affect the evacuation time of individuals and the overall outcome of the process. In addition, narrow streets and a high preference for the shortest routes may worsen the situation. This study aims to find the best evacuation route for a target population, considering less congestion in the road network and increasing the chances of reaching safe areas on time. We propose using reinforcement learning to train an intelligent network of agents, placed at the intersections, in charge of the evacuation process to fully complying evacuee agents. The model rewards decisions that lead to successful evacuation, considering the dynamics of departure times and street congestion throughout the simulation. We demonstrate the applicability of reinforcement learning to guide tsunami evacuation in a simulation and test this against a non-guided case where evacuees move following the shortest paths. Results show that the reinforcement learning model yields better outcomes than evacuations following the shortest paths.

1. Introduction

Societies implement various risk reduction strategies to mitigate the effects of large-scale disasters [1,2]. These include zoning [3], building codes, and land-use planning [4,5]. Additionally, measures such as the development of evacuation plans, increasing insurance coverage, and infrastructural improvements [6,7], along with the early detection of affected areas for disaster relief [8,9], enhance community resilience and disaster preparedness [10,11].

This study focuses on optimizing evacuation processes through evacuation models, particularly for tsunami disasters. These models are crucial in estimating the time required to move at-risk populations to shelters [12,13]. While traditionally, it is assumed that evacuees follow the shortest path to their destinations, this assumption, though often reasonable, is challenging to verify and may not always capture the dynamic nature of human behavior during crises. Evacuation decisions are made individually but are most effective when coordinated collectively, emerging from the interactions of individual choices. Studies indicate that evacuees often move in groups, influencing evacuation dynamics [14]. Group behaviors, including *tendenko* — where individuals act independently but in a similar direction [15] — can affect evacuees' overall speed and anxiety levels [16].

* Corresponding author.
E-mail address: lmoya@pucp.edu.pe (L. Moya).

https://doi.org/10.1016/j.ijdrr.2024.105023
Received 22 May 2024; Received in revised form 14 November 2024; Accepted 26 November 2024

Available online 2 December 2024

Given the primary goal of tsunami risk reduction — saving lives — improving evacuation plans is vital. Experts and authorities strive to enhance these plans based on lessons from past disasters. For instance, vehicle-based evacuations have sometimes led to delays due to traffic congestion, increasing fatalities [17]. In contrast, communities that evacuate on foot, particularly in small, tightly-knit areas, face overcrowding and narrow pathways, underscoring the need to optimize evacuation routes to alleviate congestion and ensure timely shelter access [18].

Recent reinforcement learning (RL) advancements have significantly influenced evacuation strategies, particularly in dynamic and unpredictable environments [19,20]. RL is a machine learning paradigm in which an agent learns to make effective decisions through interactions with an environment. Unlike simple repetitive simulations, RL enables agents to adapt and improve their decision-making over time by using feedback from past experiences. At each step, the agent observes the current state of the environment, which includes all relevant information, such as its position and nearby conditions. Based on this observed state, the agent selects an action from a set of possible actions and receives a reward that reflects the immediate outcome of that action. The primary objective of RL is to learn a policy — a strategy for choosing actions — that maximizes cumulative rewards over time. By experimenting with different actions and adjusting based on the rewards received, the agent progressively refines its policy, learning to make more effective decisions in future states. This continuous learning process enables the agent to develop optimal or near-optimal behavior for complex environments. This approach goes beyond traditional optimization or Monte Carlo methods by incorporating a structured feedback loop, allowing the agent to generalize from its experiences and improve its performance iteratively.

In the context of tsunami evacuation, the RL framework allows pedestrian agents to adapt to the unpredictable conditions of an emergency continuously. For example, as congestion forms along certain routes due to high pedestrian density, agents learn to adjust their paths to avoid delays, thus improving their chances of reaching safety. Additionally, this learning-based approach helps agents identify alternative routes if their preferred path becomes compromised, whether due to crowding or environmental changes caused by the tsunami. By responding dynamically to real-time conditions, the RL framework might enhance collective evacuation efficiency that not only ensures individual safety but also alleviates congestion along critical evacuation corridors. This capability is essential in high-stakes tsunami scenarios, where every second counts and agents must respond to the evolving landscape.

Yao et al. [21] used RL to reproduce real behavior during evacuation by processing crowd motion from video data. In their study, a state was defined only by the individual's coordinates — a bi-dimensional space — and did not consider more information available from the environments, such as the presence of other individuals. Furthermore, the reward assigned to the individuals depended on their distance from the targets, which might not be feasible in tsunami evacuation as there are many potential targets. Xue et al. [22] also used information from video-cameras. However, rather than reproduce real pedestrian behavior, RL was used to set an evacuation guidance system in complex structures like shopping malls and office buildings. The authors proposed a centralized system where a master agent learns and adjusts the building's evacuation strategy in real-time. In their model, a state is an image of the whole environment at a certain time, which may limit the size of the study areas. Furthermore, only a negative reward of -1 is used each time step. That is, successive arrivals to the target point are not reinforced with a positive reward. Sharma et al. [23] faced the fire evacuation building problem using RL. Instead of a bi-dimensional space, the authors adopted a graph to represent the environment, with nodes representing rooms and hallways and the edges the paths connecting the rooms and hallways. A vector with the number of people in each room was used as the state. The action of an agent is moving a person from one room to another. Thus, the set of possible actions is the number of rooms squared. The proposed model might not be convenient for tsunami evacuation studies. While building layouts and urban transportation networks can be modeled using graphs, the structure of buildings typically results in fewer nodes. On the other hand, urban networks are represented by a large number of nodes, reflecting the numerous intersections and transit hubs. As a consequence, Sharma et al. [23]'s model would have a set of actions with a large cardinality. The use of graphs to represent the transportation network was not limited to human transportation. [24] used RL for packet routing in communication networks, where the objective was to move a packet of information between nodes with the least time. Unlike human evacuation, only one packet of information can be transferred between adjacent nodes. Thus, the notion of congestion is different. Tian and Jiang [25] applied RL to determine optimal escape routes during tunnel fires, aiming for a Nash equilibrium among multiple routes. In their model, however, the total number of evacuation routers is known in advance, and the agents cannot change an evacuation route once the route is chosen. Li et al. [26] proposed an RL-based routing algorithm for large street networks during floods. In their model, a graph represents the street network. An arbitrary state contains the agent's current node position, the target node, and flood depth. However, the proposed method implies the destination node is known in advance, which is not true during tsunami evacuation. Furthermore, congestion in the network was not taken into account.

This study aims to develop a reinforcement learning (RL) based evacuation model to optimize evacuation from tsunami-prone areas into nearby shelters. Unlike most studies, we aim to implement RL over a large environment representing a complex road/street network. Another relevant difference with other studies is that there is a set of destination nodes a pedestrian needs to choose, which may change under different states. Furthermore, instead of enhancing pedestrians' capabilities to learn how to arrive at a safe area, we opt for a more directive strategy in which evacuee agents remain reactive and comply with instructions from strategically placed node agents. The manuscript is organized as follows: Section 2 describes the RL framework and our evacuation model. Section 3 assesses the method in two experiments. Further discussion of the proposed method is reported in Section 4. Finally, our conclusion is conveyed in Section 5.

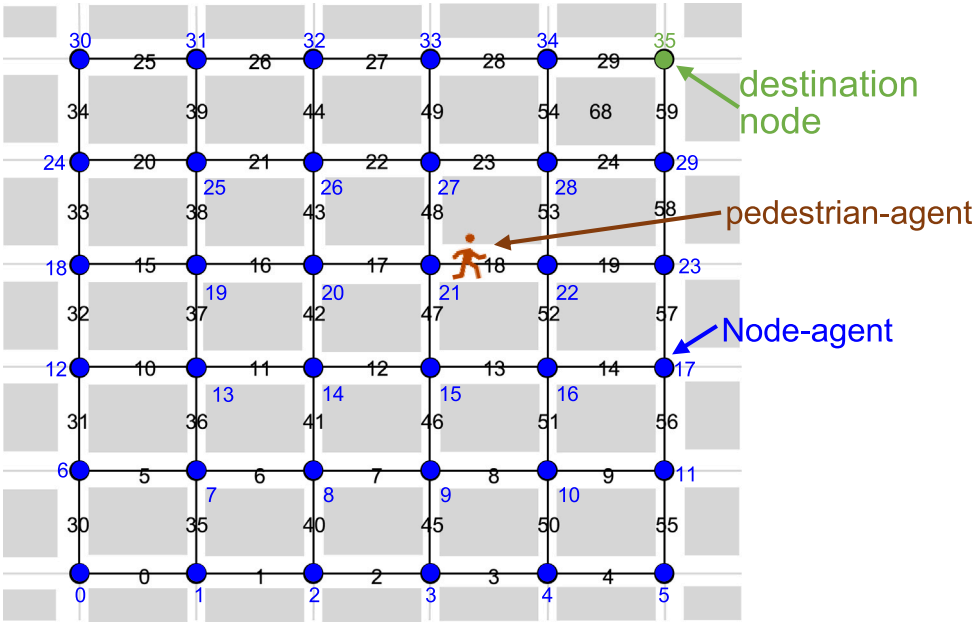

Fig. 1. Illustration of an environment consisting of 36 nodes, 60 edges, and one pedestrian agent.

2. Methodology

This section outlines the fundamental concepts for calibrating an RL-based evacuation guidance system. First, we describe the system's environment, comprising synthetic pedestrians and a transportation network. In this setup, pedestrians interact with and navigate the network to reach safety. Subsequently, we define the learning process to determine the optimal evacuation routes. It is important to note that this learning process is embedded within an agent-based modeling framework. This approach involves a computational model that simulates the behaviors and movements of individual entities, referred to as agents, during an evacuation.

2.1. Environment

The *environment* encompasses all the physical entities and agents involved in the evacuation process. A critical component is the *transportation network*, through which pedestrians navigate. This network is modeled as a graph, where roads and streets are represented by a set of edges $\mathcal{E}$, and intersections by a set of nodes $\mathcal{N}$. An edge $e_i \in \mathcal{E}$ is defined by the nodes at its ends and the width of the corresponding road or street, denoted as $e_i = (n_j, n_k, w_i)$, where $\{n_j, n_k\} \in \mathcal{N}$ and $w_i \in \mathbb{R}$. The width w_i is assumed uniform across the entire edge. Additionally, a node $n_i \in \mathcal{N}$ is characterized by its position vector $\mathbf{x}_i$, and a binary value b_i, such that $n_i = (\mathbf{x}_i, b_i)$, where $\mathbf{x}_i \in \mathbb{R}^2$ represents a bidimensional vector and $b_i \in \{0, 1\}$. The binary value b_i signifies whether n_i is a destination, with 1 indicating a destination node and 0 an evacuation node. A destination node may be near a structure designed for protection, like vertical evacuation buildings for tsunamis or outside the hazardous area that pedestrian agents are fleeing [27,28]. On the other hand, evacuation nodes are located inside the hazardous area and are part of a potential evacuation route. For the sake of brevity, evacuation nodes will be referred to as nodes.

An illustration of the transportation network model is shown in Fig. 1. In this figure, edge indices are colored black, while node indices are color-coded: blue for evacuation nodes and green for destination node. Additionally, we introduce the operator $B(e_i) = \{n_j, n_k\}$, which represents the end nodes of edge e_i. Similarly, the operator $C(n_i) = \{e_j \mid n_i \in B(e_j)\}$ denotes the subset of edges adjacent to node n_i. For example, in Fig. 1, $B(e_{55}) = \{n_5, n_{11}\}$ and $C(n_{29}) = \{e_{24}, e_{58}, e_{59}\}$.

Another component of the environment is the set of pedestrian agents, $\mathcal{P}$, representing the population seeking destination nodes. Each pedestrian-agent $p_i \in \mathcal{P}$ is defined by four parameters: $p_i = (\mathbf{y}_i, \mathbf{v}_i, t_i, s_i)$. Here, $\mathbf{y}_i \in \mathbb{R}^2$ denotes the agent's position vector, $\mathbf{v}_i \in \mathbb{R}^2$ represents its velocity vector, $t_i \in \mathbb{R}$ indicates the evacuation departure time, and $s_i \in \{0, 1\}$ is a binary parameter indicating whether the pedestrian-agent has reached a destination node ($s_i = 1$) or is still moving towards one ($s_i = 0$). It is important to note that these parameters can depend on additional user-defined factors. For example, $\mathbf{v}_i$ may vary with the age and the pedestrian-agent density at $\mathbf{y}_i$. Similarly, t_i could be modeled as a random variable distributed according to a specific function, reflecting the varied times at which pedestrian agents begin their evacuation—this is not necessarily synchronized with the start of the simulation. Additionally, the initial position for evacuation, such as a home or workplace, might vary depending on the time of day.

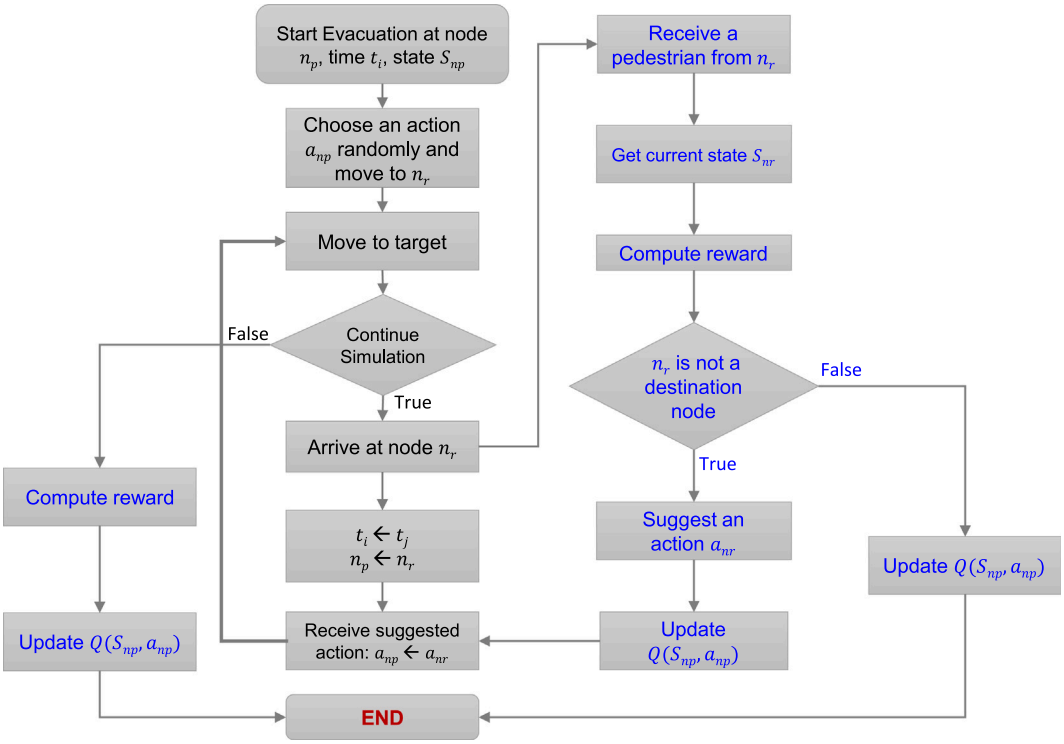

Fig. 2. Flowchart of the interaction between a pedestrian-agent and node agents. Actions performed by the pedestrian-agent are colored black, whereas actions performed by the node-agents are colored blue. (For interpretation of the references to color in this figure legend, the reader is referred to the web version of this article.)

2.2. Learning process

The primary goal of this system is to guide the evacuation process for pedestrian agents. To achieve this, a new type of agent, termed *node-agent*, is introduced. A node-agent is stationed at each node within the network. Upon the arrival of a pedestrian-agent at a node, the node-agent directs which edge in the evacuation route to take next. A node-agent, n_i can only access information from the edges in $C(n_i)$. According to Sutton and Barto [29], a *state*, hereafter referred to as S, encompasses all the perceivable environmental information at a specific moment. In the specific context of our problem, a state S is defined by a node n_i, the set of edges $C(n_i)$ connected to it, and the pedestrian agents present at these edges. As a state is spatially linked to a node, S_{n_i} is hereafter referred as the state observed at node n_i. Depending on S_{n_i}, the possible actions $\mathcal{A}(S_{n_i})$, are the edges a pedestrian-agent can take to keep evacuating, that is, $\mathcal{A}(S_{n_i}) = C(n_i)$.

In the reinforcement learning (RL) framework applied here, rewards are used to guide pedestrian-agents toward safer and more efficient evacuation routes by providing feedback on their actions. The *reward* concept is introduced as a measure assigned to a pedestrian-agent based on the safety and efficiency outcomes of its actions. Consider the following sequence of events (Fig. 2): (i) at time t_i, a pedestrian-agent arrives at node n_p and observes state S_{n_p}, (ii) the agent takes action $a_{n_p} \in \mathcal{A}(S_{n_p})$, selecting an edge to proceed, and (iii) at time t_j, the agent reaches node n_r, enters a new state S_{n_r}, and receives a reward R_{t_j}, reflecting the impact of its choice. The reward associated with state S_{n_p} and action a_{n_p} is determined by the outcome at S_{n_r}. Specifically, if n_r is a *destination* node (meaning the pedestrian-agent has reached safety), a positive reward R^{safe} is given to reinforce the successful evacuation. In contrast, if n_r is not a destination node, indicating that the agent remains in a potentially hazardous area, a negative reward R^{unsafe} is assigned. This negative reward is proportional to the time elapsed $(t_j - t_i)$, penalizing slower, less efficient routes. Additionally, if a pedestrian-agent has not reached a destination node by the end of the simulation, it incurs an extra negative reward R^{harm}, which represents the risk associated with remaining in the evacuation area. These positive and negative rewards are designed to incentivize safe and timely evacuation, with positive rewards reinforcing actions that lead to safety and negative rewards discouraging delays or unsafe paths. This structure encourages agents to prioritize actions that reduce their overall time in risky zones, thereby improving both individual and collective outcomes over the course of the simulation.

Recall that a reward quantifies the outcome of a single action. It is also necessary to quantify the sequence of actions that lead a pedestrian-agent from any node agent to either a destination node or an unsuccessful evacuation. Thus, the *return* is introduced as a cumulative reward to assess the long-term effects of an arbitrary pedestrian agent's actions and is defined as follows:

$$\begin{aligned} G_{t_0} &= R_{t_1} + \gamma R_{t_2} + \gamma^2 R_{t_3} + \cdots + \gamma^{T-1} R_{t_T} \\ &= \sum_{k=0}^{T-1} \gamma^k R_{t_{k+1}} \end{aligned} \tag{1}$$

where G_{t_0} represents the total return starting when a pedestrian-agent receives guidance from an arbitrary node-agent at time t_0; $t_1, t_2, \ldots, t_{T-1}$ denote the times when the pedestrian-agent interacts with subsequent node-agents; t_T is the time when the pedestrian-agent either reaches a destination node or the simulation ends; and $\gamma < 1$ represents the *discount rate*, which values rewards received earlier higher than those received later. This formulation helps evaluate the effectiveness of sequential decisions leading to safety or continued risk. The expected return at t_i, when the state $S_{n_p} = s$ and the action $A_{n_p} = a$, is defined as the *action-value* function:

$$q(s,a) = \mathbb{E}[G_{t_i} | S_{n_p} = s, A_{n_p} = a] \ , \ \forall a \in \mathcal{A}(s) \tag{2}$$

where $\mathbb{E}$ denotes the expected value operator. If the action-value function for each possible action is known, the optimal decision is the action associated with the highest $q(s,a)$:

$$q^*(s,a) = \max_{a \in \mathcal{A}(s)} q(s,a) \tag{3}$$

Therefore, the computation of the action-value functions is the primary objective in the learning process. In this study, as in most applications of reinforcement learning, the action-value function is approximated through continuous simulations involving pedestrian agents attempting to reach a destination point. When a pedestrian-agent arrives at a node, the corresponding node-agent assigns the optimal edge to continue toward a destination point. Concurrently, the pedestrian-agent communicates to the node-agent the information obtained from the previous node-agent. The node-agent then uses this information to update the estimated action-value function, facilitating the refinement of future guidance based on past outcomes with the following expression:

$$Q(S_{n_p}, A_{n_p}) \leftarrow Q(S_{n_p}, A_{n_p}) + \alpha[R_{t_j} + \gamma Q(S_{n_r}, A_{n_r}) - Q(S_{n_p}, A_{n_p})] \tag{4}$$

where $Q(S_{n_p}, A_{n_p})$ is the approximation of the action-value for a state S_{n_p} and an action A_{n_p}, and α is the step-size parameter. The update equation, shown as Eq. (4), is derived from the SARSA method, a RL technique used to adjust $Q(S_{n_p}, A_{n_p})$ [29]. To ensure that the system experiences a wide range of states during the calibration process, node-agents utilize two distinct modes for suggesting an edge to pedestrian-agents. In the *explore* mode, a node-agent randomly selects an edge to facilitate the exploration of new states. Conversely, the *exploit* mode uses Eq. (3) to leverage the accumulated knowledge, making decisions based on the best-perceived action. The node-agent alternates between these modes based on a predetermined strategy, with the proportion of exploration governed by the ϵ parameter, often referred to as the exploration rate.

Fig. 2 synthesizes the previously introduced concepts and illustrates the interaction between an arbitrary pedestrian-agent and the node-agents. It begins when the pedestrian-agent starts the evacuation at node-agent n_p, at time t_i. The node-agent provides information on the state S_{n_p} at time t_i. Then, the pedestrian-agent choose randomly an action a_{n_p} and moves to the node-agent n_r. When the pedestrian-agent arrives at the node-agent n_r at time t_j, the state S_{n_r} and the reward R_{t_j} for the pedestrian-agent are computed. If n_r is a destination node, $R_{t_j} = R^{safe}$, the action-value $Q(S_{n_p}, a_{n_p})$ is updated using Eq. (4), and the interaction of the pedestrian-agent with the node-agents finishes. Otherwise, $R_{t_j} = R^{unsafe}$, and n_r suggest an action to the pedestrian-agent. If the suggestion is based on the explore mode, the node-agent picks the next target node randomly from $\mathcal{A}(S_{n_r})$. If the suggestion is based on the exploit mode, the agent picks the next target node using Eq. (3). After the action is chosen, Eq. (4) is used to update the action-value $Q(S_{n_p}, a_{n_p})$. Finally, the pedestrian-agent receives the suggestion and moves to the next node-agent target, and the whole process repeats. If the evacuation simulation finishes and the pedestrian-agent is still directing to a node-agent, a reward R^{harm} could be assigned, and the action value $Q(S_{n_p}, a_{n_p})$ is updated.

3. Numerical experiments

3.1. Uniform grid

The first experiment calibrates an evacuation guidance system within a uniform grid, as Fig. 1 illustrates. This grid features a single destination node, n_{35}, in the upper-right corner. The simulation incorporates 2000 pedestrian agents, initially positioned at n_0, the node at the lower-left corner. The velocity of each pedestrian-agent, denoted by $|\mathbf{v}_i|$, is calculated based on the density-dependent speed model proposed by Takabatake et al. [30], as shown below:

$$|\mathbf{v}_i| = \begin{cases} 1.19 & \text{if } \rho_i < 0.3 \\ 1.19 - (\rho_i - 0.3)(\frac{1.19-0.2}{3-0.3}) & \text{if } 0.3 \le \rho_i < 3 \\ 0.2 & \text{if } \rho_i \ge 3 \end{cases} \tag{5}$$

where $|\mathbf{v}_i|$ represents the speed of the ith pedestrian-agent, while ρ_i indicates the density of pedestrian around the pedestrian-agent's position, $\mathbf{y}_i$. We calculate the pedestrian-agent density every 2 meters along each grid edge to enhance computational efficiency. This density is then uniformly applied to all agents within that segment. The evacuation departure time for the pedestrian-agents is modeled as random variables. These times follow a Rayleigh distribution, with a mean value of 420 s (7 min) to consider human reaction and mobilization delays.

A simplified state model is used to reduce the computational load. Thus, the state at node n_i, S_{n_i}, consists of the node n_i and the pedestrian density levels observed at each edge connected to it (i.e., $c(n_i)$). The density level, d_{e_j}, denotes the maximum pedestrian density observed on edge e_j. Three distinct pedestrian density levels are considered and computed as follows:

$$d_{e_j} = \begin{cases} 0 & \text{if } \rho^{e_j} < 0.3 \\ 1 & \text{if } 0.3 \le \rho^{e_j} < 3 \\ 2 & \text{if } \rho^{e_j} \ge 3 \end{cases} \tag{6}$$

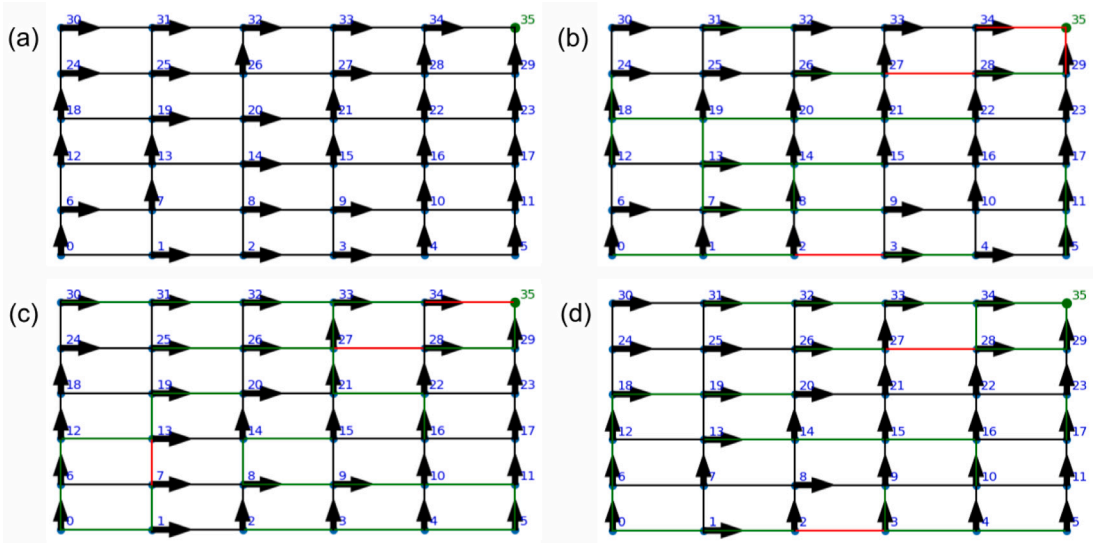

Fig. 3. Street network of the first case study under different scenarios. The colors of the edges represent pedestrian density levels, where black, green, and red denote the first, second, and third levels, respectively. Arrows indicate the system's suggested directions when a pedestrian arrives at a node under these scenarios. (For interpretation of the references to color in this figure legend, the reader is referred to the web version of this article.)

where ρ^{e_j} represents the maximum pedestrian-agent density (people/m^2) observed at edge e_j. For instance, the state at node n_{15} is represented by the array $S_{n_{15}} = (n_{15}, d_{e_{12}}, d_{e_{13}}, d_{e_{46}}, d_{e_{47}})$, illustrating the density levels at the connected edges. Similarly, the state for n_1 is described as $S_{n_1} = (n_1, d_{e_0}, d_{e_1}, d_{e_{35}})$. Recall that the states are dynamic and change over time.

Regarding the calibration process, we performed 5000 evacuation simulations, each lasting 30 min. Each simulation builds upon the accumulated knowledge from previous runs, enhancing the efficiency and accuracy of the model's predictions. In terms of the balance between the explore and exploit modes, the ϵ parameter is adjusted according to the following rule for the kth simulation:

$$\epsilon_k = \frac{1}{\frac{4k}{N} + 1} \tag{7}$$

where $N = 5000$ is the number of evacuation simulations. Note that the ϵ parameter is crucial in node decision-making. Initially, with $\epsilon_0 = 1$ during the first simulation, node agents make random decisions when guiding pedestrian agents at a node, promoting exploratory behavior. As simulations progress, this parameter is gradually reduced to $\epsilon_N = 0.2$ by the final simulation, whereby 80% of the time node-agents rely on Eq. (3) to select the most effective edge for evacuation, enhancing decision-making efficiency based on learned experiences.

Upon completing the calibration process, the optimal evacuation routes for various scenarios are illustrated in Fig. 3, with arrows indicating these paths. Edge density levels are color-coded—black for level 0, green for level 1, and red for level 2. Fig. 3a shows the preferred paths when density level 0 prevails. Notably, as density levels change, the arrows' directions also change. The nodes n_{27} in Figs. 3b–d and n_7 in Figs. 3b and 3c, are such examples that reflect adaptive routing to manage congestion.

Fig. 4 charts pedestrian agents' progress toward the destination node over time. Initially, only 586 agents reached the destination node after the first simulation, but this number climbs to 1881 after ten simulations and reaches complete evacuation by the 100th simulation. Over the following simulations, the evacuation process accelerates significantly, as demonstrated by the curve from simulation number 5000, which outpaces earlier simulations. This improvement is primarily attributed to the system's ability to reduce congestion, thereby maintaining higher velocities among the pedestrian agents and reducing negative rewards. Moreover, Fig. 4 compares this performance against a scenario where all agents follow the same shortest path, calculated using the Dijkstra algorithm [31]. The results indicate that the RL-based guidance system consistently outperforms the shortest path strategy, with the most notable difference being the evacuation of an additional 529 pedestrian agents at approximately 810 s.

3.2. Tsunami evacuation at the city of Kochi, Japan

The proposed method was applied to the tsunami evacuation of a portion of Kochi city, Japan, to test the system under realistic conditions. This scenario is based on a potential magnitude Mw 9.1 earthquake from the anticipated Nankai Trough scenarios, as outlined in Case 4 by the Cabinet Office of Japan, with the projected inundation area shown in Fig. 5 [32–35]. The urban road network modeled comprises 2733 nodes and 3426 edges, reflecting the complex topology of the city's infrastructure. In this scenario, 48 nodes close to government-designated tall buildings, officially recognized for vertical evacuation, serve as destination nodes. This choice of locations is pivotal, given their structural integrity and accessibility in flood scenarios. The simulation deploys 40,995 pedestrian agents, uniformly distributed across the nodes, to evaluate the efficiency and robustness of the evacuation routes.

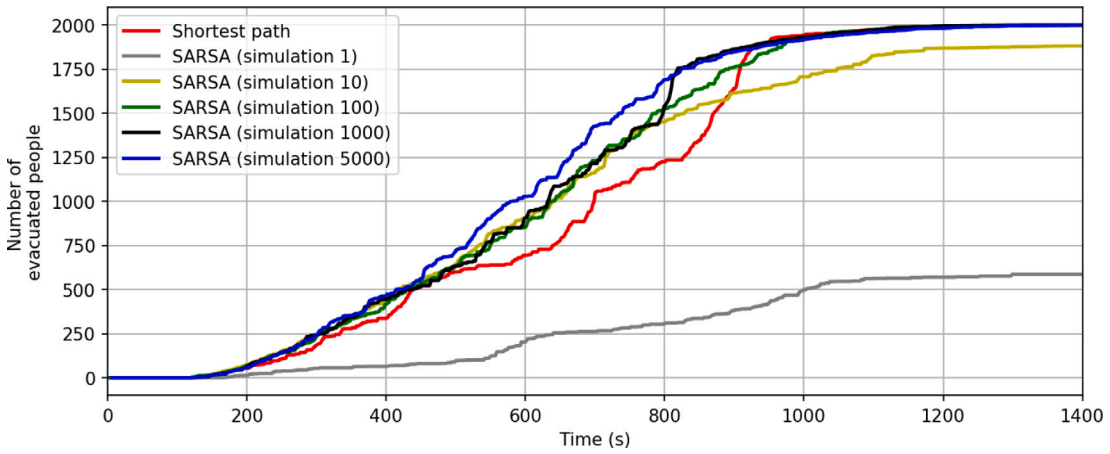

Fig. 4. Number of evacuated people vs time of the first numerical experiment. The red line denotes the results using Dijkstra-based shortest path [31]. In contrast, the gray, yellow, green, black, and blue lines are the results using the SARSA algorithm after 1, 10, 100, 1000, and 5000 evacuation simulations. (For interpretation of the references to color in this figure legend, the reader is referred to the web version of this article.)

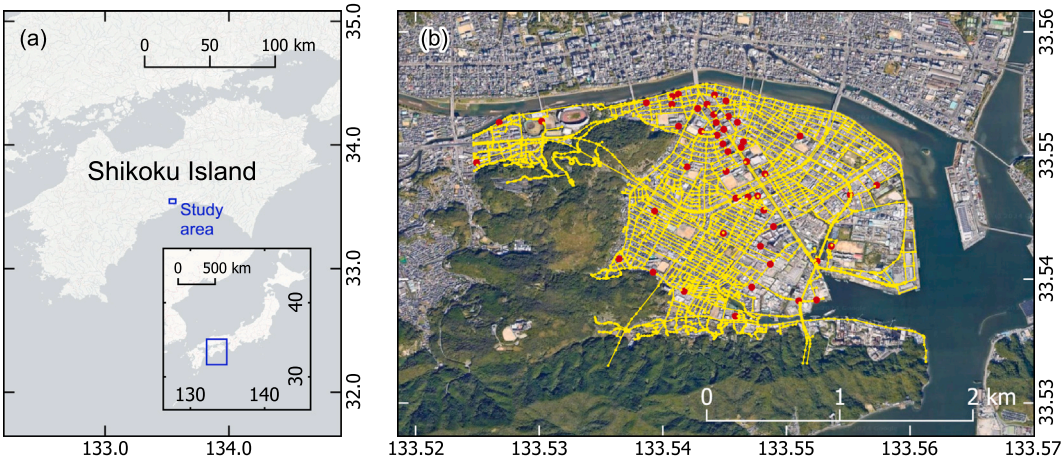

Fig. 5. (a) Location of the second study area in Shikoku Island. The inset shows the location of Shikoku Island in Japan. (b) Closer view of the second study area. The yellow lines depict the road network, and the red dots denote the location of evacuation points. (For interpretation of the references to color in this figure legend, the reader is referred to the web version of this article.)

The pedestrian agents' behavior and the vector representation of states in the Kochi tsunami evacuation scenario are modeled similarly to the uniform grid experiment in Section 3.1. The model considers three density levels for each edge as previously established (Eq. (6)) and discretizes edges into approximately 2-meter intervals. Pedestrian density and velocity are recalculated at these intervals every 10 s (Eq. (5)), facilitating a dynamic response to changing conditions during the simulation. The initiation of evacuation is modeled with a Rayleigh distribution, now using a mean value of 300 s (5 min) to reflect the urgent nature of tsunami evacuations. A discount rate of $\gamma = 0.9$ is applied to calibrate the action value functions, emphasizing the importance of immediate rewards in a high-stakes evacuation scenario. To ensure robustness in our results, the calibration involved 11,000 simulations, with adjustments to the learning rate ϵ as defined in Eq. (7).

After 11,000 simulations, the number of pedestrian agents evacuated over time is depicted in Fig. 6. The performance of the shortest path method is also shown as a red line. In these experiments, the reinforcement learning approach excels over the shortest path method during the initial 16 min, achieving its most significant advantage with 3012 more evacuated pedestrians at about $t = 520$ s. The difference is primarily due to the reinforcement learning method's adaptability to high pedestrian densities, which occur early in the evacuation due to the Rayleigh distribution of starting times, with a mean of 300 s (Fig. 7). The initial minutes are critical due to edges experiencing high pedestrian densities, where the reinforcement learning-based evacuation routes prove to be more effective than the shortest path method. However, as pedestrian density diminishes, the shortest path approach gradually becomes more viable, demonstrating its effectiveness in less congested conditions. The evacuation routes suggested by the guidance system to some pedestrian-agents are reported in Fig. 8. Note that even from the same starting position, different routes have been suggested, with many ending up at different destination nodes. That is, the system made different suggestions under different

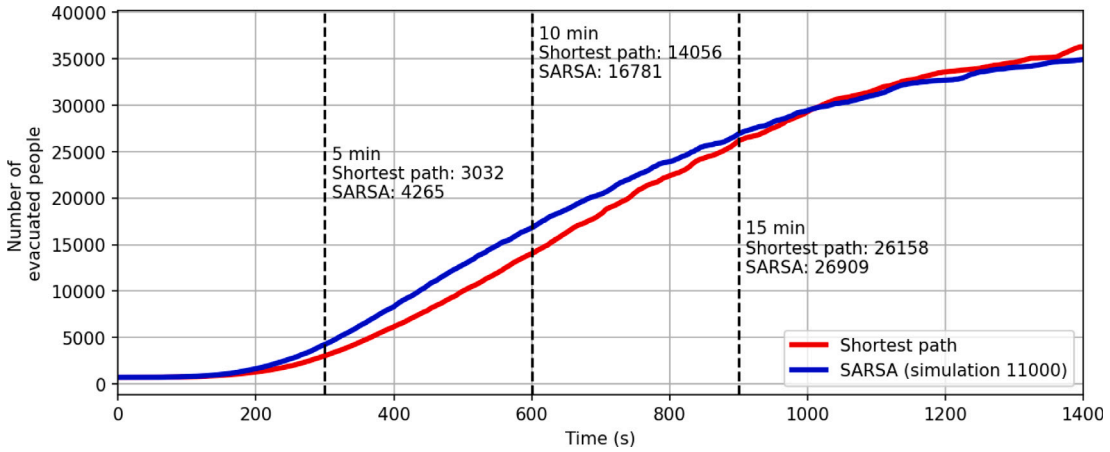

Fig. 6. Number of evacuated people vs time of the second numerical experiment. The red line denotes the results using Dijkstra-based shortest path [31], whereas the blue line uses the SARSA algorithm after 11000 evacuation simulations. The black vertical dashed lines are located at times 5 min, 10 min, and 15 min. (For interpretation of the references to color in this figure legend, the reader is referred to the web version of this article.)

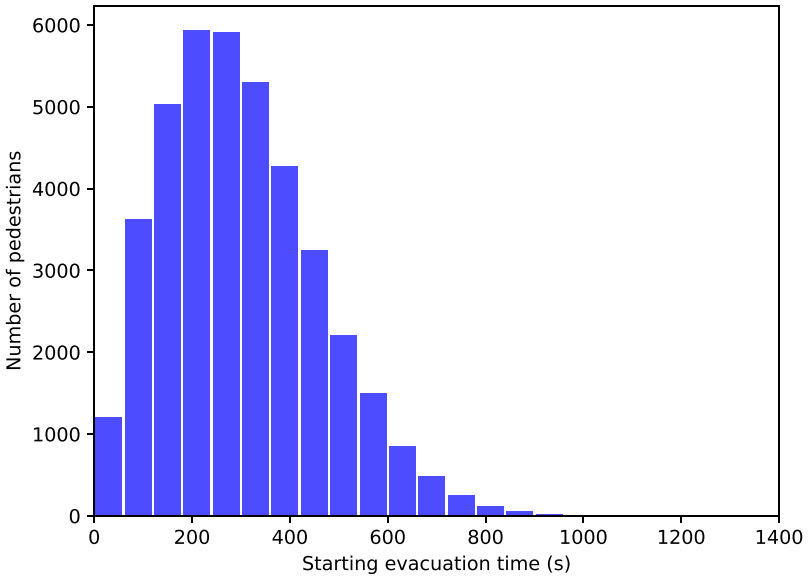

Fig. 7. Distribution of 40,995 pedestrian agents according to their starting evacuation time. A Rayleigh distribution with 300 s as the mean value is used.

conditions regarding the density of pedestrians at the edges. A closer examination of the travel times for the entire set of pedestrian-agents (Fig. 9) shows that while some pedestrians experienced shorter travel times using the SARSA algorithm, others encountered longer travel times. However, as mentioned above, during the initial minutes, a larger proportion of pedestrian-agents benefited from a significant reduction in travel time with the SARSA algorithm. These results suggest that the SARSA algorithm optimizes for improvements in collective behavior rather than focusing on the individual behavior of pedestrians.

4. Discussion

This study proposes using RL to calibrate an evacuation guidance system aimed at aiding pedestrians in evacuating areas soon to be impacted by a tsunami. Results show that the guidance system improves evacuation efficiency during the initial minutes when congestion commonly occurs on roads due to high pedestrian density. This improvement is critical in scenarios where tsunamis arrive shortly after an earthquake. For instance, in Palu City, Indonesia, a tsunami struck merely six minutes after an

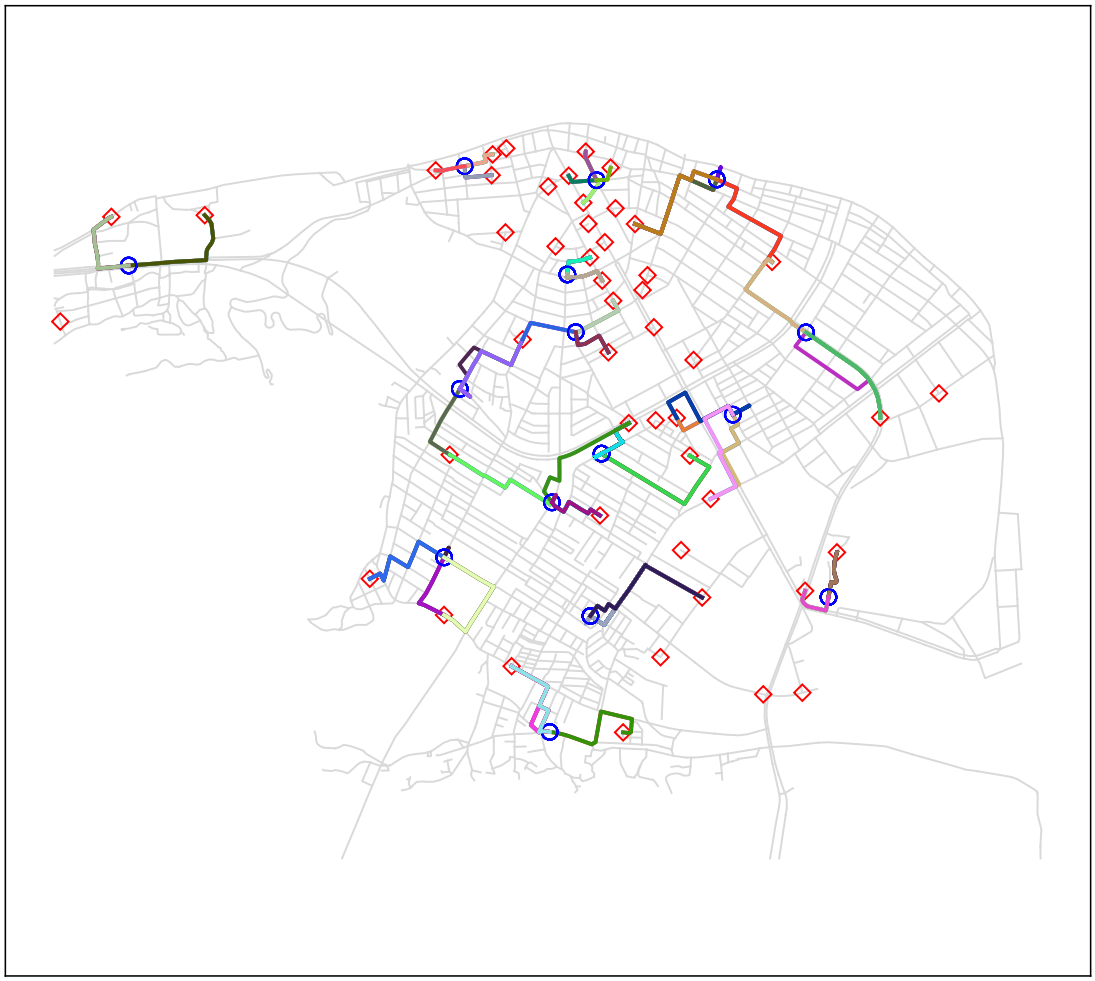

Fig. 8. Illustration of some pedestrians paths. Red diamond marks show the location of destination nodes. Blue circle marks show the location of some node-agents, and the colored lines denote all the pedestrian's paths from the blue marks to a destination node observed during the evacuation process under the guidance system. The gray lines represent the transportation network. (For interpretation of the references to color in this figure legend, the reader is referred to the web version of this article.)

earthquake [36]. Similar cases include Padang, Indonesia [37], Puerto Angel, Mexico [38], Camana, Peru [39], and Iquique and Valparaiso, Chile [40,41].

In certain areas, however, a slightly longer tsunami arrival time is anticipated. In Peru, for example, simulations estimate a tsunami arrival time of about 20 min in El Callao [28,42] and 21 min in Marcona [43]. Likewise, Tumaco, Colombia, has an estimated tsunami arrival time ranging from 20 to 35 min [44]. Yet, even in these cases, the effective evacuation time can be influenced by the timing of tsunami warnings, which varies with local seismic network density. Japan, for example, is among the most prepared nations, capable of issuing tsunami alarms within three minutes [45]. However, this rapid response is not universal. In high seismic network density areas, the National Oceanic and Atmospheric Administration (NOAA) in the USA estimates a warning time of around five minutes, whereas in regions with lower network density, this time can extend to 10–15 min [46]. In Peru, the National Centre for Tsunami Alerts expects to issue warnings within approximately 24 min [47]. For this reason, communities vulnerable to tsunamis projected to arrive in less than 30 min are advised to begin evacuation immediately after ground shaking ceases [48–52]; however, the 2011 Tohoku-Oki earthquake in Japan showed that citizens preferred to wait for an official warning [53]. Under these circumstances, this study demonstrates that applying RL for pedestrian guidance may increase the number of survivors in the aftermath of a large-scale tsunami. By reducing congestion and facilitating more efficient movement, the RL-based guidance system can significantly alleviate bottlenecks along critical evacuation routes, thus allowing more individuals to reach safe zones in a shorter time frame. Increased survival rates also mean that fewer resources are needed for immediate rescue efforts, enabling authorities to focus on post-disaster recovery.

It is important to clarify the assumptions of our model, as they are intended to balance the complexity of real-world evacuation with the specific objectives of this study. For example, the velocity of the pedestrian agents in our model is determined by the local

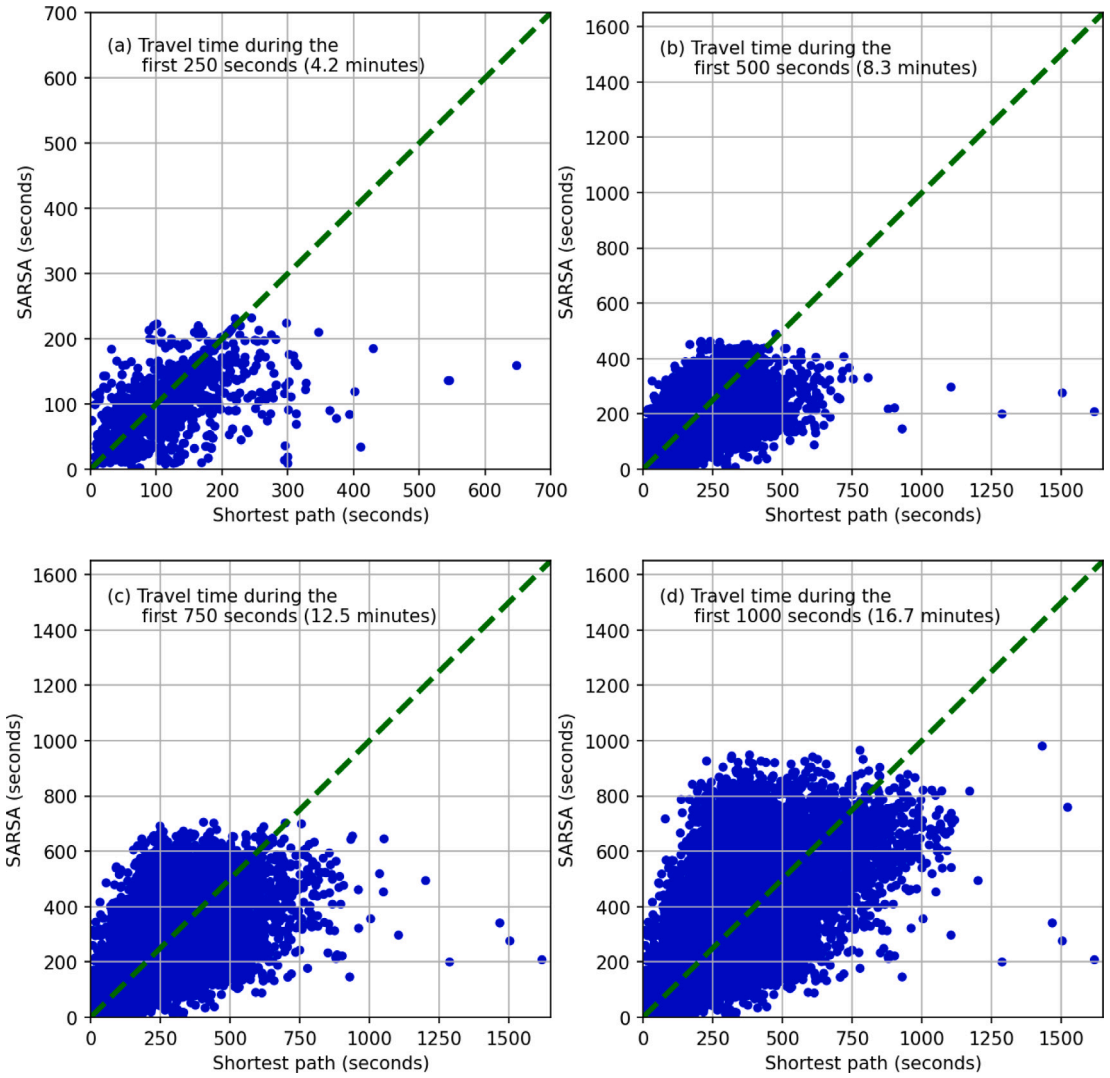

Fig. 9. Pedestrian's travel times using the SARSA algorithm vs that using the shortest path approach. Results are reported during the first (a) 250 s, (b) 500 s, (c) 750 s, and (d) 1000 s. The green dashed line denotes equal travel times between the two approaches. (For interpretation of the references to color in this figure legend, the reader is referred to the web version of this article.)

pedestrian density. However, walking speed is influenced by various other factors, including age and ground slope. Future studies could incorporate these variables to capture these nuanced effects on pedestrian velocity more accurately. For instance, Chen et al. [54] adopted a walking speed as a function of ground slope. Pedestrian age should also be considered in further studies. To further simplify decision-making in our RL framework, pedestrian agents in this study make directional decisions only upon reaching nodes. In real-world situations, however, individuals make continuous decisions based on their surroundings. Despite these controlled conditions, it is essential to emphasize that our model provides a foundational guidance system rather than enforcing a specific route choice, which allows for a clear evaluation of RL effectiveness. Another simplification in the experimental evaluations was assuming all nodes are on a horizontal plane, ignoring topography. This assumption could be addressed by incorporating three-dimensional coordinates for the nodes. A more critical simplification concerns the departure time of the pedestrian agents. Commonly, there is a delay between the issuance of an early warning and the initiation of evacuation. The time delay components are reported in Chen et al. [55]. The lack of conclusive evidence on the distribution of this delay poses a challenge. For this study, we adopted the Rayleigh distribution based on our previous experiences with tsunami disasters and evacuation modeling studies [13,56–58]. However, other studies suggest that the departure time distribution has a larger variance than a Rayleigh distribution [59,60]. Overall, these simplifications allow us to isolate and evaluate the benefits of RL over traditional shortest-path methods in controlled conditions. They enable us to demonstrate that RL improves evacuation flow during initial stages under crowding conditions. Further

integration of detailed factors such as age and topography will allow this RL-based framework to be adapted more directly to specific real-world evacuation scenarios.

An essential consideration in the RL framework is the selection of positive and negative reward values. Ensuring that the rewards are structured to promote effective evacuation behavior is crucial. A positive reward is granted when a pedestrian agent reaches a destination node. At the same time, a negative reward is applied at each simulation step and, potentially, at the end of the simulation. We recommend setting the reward values such that the total return experienced by a pedestrian agent who successfully reaches a destination node remains positive; this can be mathematically expressed as:

$$N^{step} \times R^{unsafe} + R^{harm} \ll R^{safe} \tag{8}$$

where N^{step} represents the number of steps in a simulation. This inequality ensures that the cumulative negative rewards (from unsafe conditions and potential harm) are significantly lower than the positive rewards for reaching safety.

Additional comments regarding the challenges encountered during the calibration of the guidance system are necessary. Nodes with low connectivity, denoted as $\#C(n) = 1$ or 2, and situated far from destination nodes, required more simulations to yield coherent guidance for the pedestrian agents. The predominant observation was that pedestrian agents moved within closed loops around these nodes after several simulations. This phenomenon primarily arises due to the low connectivity, resulting in few pedestrian agents traversing these nodes. Moreover, as these nodes are distant from evacuation nodes, only a smaller fraction of pedestrians manage to reach a destination node and receive a positive reward. Therefore, to speed up the calibration process, it is advisable to initially place a higher number of pedestrian agents at nodes with low connectivity during the simulation. Then, after the calibration process is done, these additional pedestrians should not be included in a simulation to estimate an actual evacuation behavior.

In the experiment for the City of Kochi in Section 3.2, pedestrian agents were initially distributed uniformly across the set of nodes. This setup may result in certain evacuation nodes never experiencing high pedestrian densities, even though these nodes might represent densely populated areas in real-world scenarios. However, uniform distribution ensures that all nodes are exposed to a range of states, which may not occur if actual population density were used. To address this, for calibrating the guidance system, we propose augmenting the uniform distribution by adding additional pedestrian agents according to the population density distribution of the area of interest. In cases where population density data is unavailable, extra pedestrians could be assigned to a randomly selected subset of nodes to simulate potential crowding conditions. For simulating actual evacuation behavior, and after the system has already been calibrated, the real distribution of pedestrians should be used.

Implementing the proposed method in a real-world tsunami emergency could present challenges if traditional traffic management systems are relied upon. One key limitation is that, at each intersection, traffic management would require the installation of sensors capable of detecting the number of pedestrians on roads or in alleys, which would be more costly and complex compared to deploying static metal signs. Moreover, installing and maintaining such infrastructure may not be feasible in many regions, particularly those vulnerable to disasters. However, modern technology offers more practical alternatives. By leveraging the widespread use of mobile devices, it becomes feasible to track and monitor pedestrian movement in real time. Through mobile phone data and digital communication networks, authorities can collect real-time information about the locations of evacuees within the transportation network. A recent study has shown that GNSS installed in mobile phones can be used to guide pedestrians during evacuation drills [61]. This digital approach not only reduces costs associated with hardware installation but also provides greater flexibility and adaptability during dynamic emergency situations.

5. Conclusions

We have developed a model based on reinforcement learning to enhance evacuation for areas at risk of being inundated by a tsunami. This model operates within a virtual environment, where a network of edges and nodes represents the urban infrastructure, and evacuees are simulated as pedestrian agents. Directions are provided to these agents by other agents located at the network's nodes (i.e., the node agents), utilizing principles of reinforcement learning. The proposed method's effectiveness was tested in two scenarios: a simple grid network with 5,000 pedestrian agents and a more complex scenario representing the city of Kochi, Japan. The results indicate that our model surpasses traditional shortest path-based evacuation strategies, particularly in the initial phases of evacuation—within the first 900 and 1,000 s for the respective cases. The most significant improvement observed was an increase in evacuated individuals by 529 (40%) in the first scenario and by 3,012 (7%) in the second.

In the aftermath of a large-magnitude earthquake with an offshore epicenter, a tsunami may impact coastal cities within minutes. Efficiently evacuating the population from areas likely to be affected by the tsunami remains a pressing challenge. Thus, this study contributes to strategies for effectively evacuating more people in the crucial initial minutes following such events.

CRediT authorship contribution statement

Erick Mas: Writing – original draft, Visualization, Validation, Supervision, Software, Resources, Project administration, Methodology, Investigation, Funding acquisition, Formal analysis, Conceptualization. **Luis Moya:** Writing – original draft, Visualization, Validation, Supervision, Software, Resources, Project administration, Methodology, Investigation, Funding acquisition, Formal analysis, Data curation, Conceptualization. **Edgard Gonzales:** Writing – original draft, Visualization, Investigation, Conceptualization. **Shunichi Koshimura:** Validation, Supervision, Resources, Project administration, Investigation, Funding acquisition, Conceptualization.

Declaration of competing interest

The authors declare the following financial interests/personal relationships which may be considered as potential competing interests: Luis Moya reports financial support was provided by National Council of Science Technology and Technology Innovation, Peru. Shunichi Koshimura reports a relationship with Japan Society for the Promotion of Science that includes: funding grants. If there are other authors, they declare that they have no known competing financial interests or personal relationships that could have appeared to influence the work reported in this paper.

Acknowledgments

This study was funded by CONCYTEC-PROCIENCIA of Peru (Contract No. PE501078853-2022) and the SIP program (Cross-ministerial Strategic Innovation Promotion Program) of the Cabinet Office, Japan (Grant 23814135). We also acknowledge the JSPS Kakenhi Programs (Grant 21H05001), JST Japan-US Collaborative Research Program (JPMJSC2311). The authors thank the Core Research Cluster of Disaster Science at Tohoku University (a Designated National University) for their support.

Data availability

Data will be made available on request.

References

[1] N. Shuto, K. Fujima, A short history of tsunami research and countermeasures in Japan, Proc. Japan Acad. Series B 85 (8) (2009) 267–275, http://dx.doi.org/10.2183/pjab.85.267.
[2] L. Ceferino, Y. Merino, S. Pizarro, L. Moya, B. Ozturk, Placing engineering in the earthquake response and the survival chain, Nature Commun. 15 (1) (2024) 4298.
[3] Washington State Department of Natural Resources, Tsunami design zone maps for washington state building code, 2021, available at https://www.dnr.wa.gov/wa-tdz#2021-tsunami-design-zone. (Online; Last Accessed 15 May 2024).
[4] J. León, A. March, Urban morphology as a tool for supporting tsunami rapid resilience: A case study of talcahuano, Chile, Habitat Int. 43 (2014) 250–262.
[5] M. Garcia-Fry, O. Murao, S. Bachri, L.A. Moya, Land-use microsimulation model for livelihood diversification after the 2010 Merapi volcano eruptions, Transp. Res. D: Transp. Environ. 104 (2022) 103189.
[6] K. Hammad, I. Lotfy, M. Naiem, Enhancing progressive collapse resistance in existing buildings, in: I. El Dimeery, M. Baraka, S.M. Ahmed, A. Akhnoukh, M.B. Anwar, M. El Khafif, N. Hanna, A.T. Abdel Hamid (Eds.), Design and Construction of Smart Cities, Springer International Publishing, 2021, pp. 39–46, http://dx.doi.org/10.1007/978-3-030-64217-4_5.
[7] R.P. Clarke, Natural disaster mitigation using advanced ferrocement – Future research directions for improved building resilience, Case Stud. Construct. Mater. 16 (2022) e00990, http://dx.doi.org/10.1016/j.cscm.2022.e00990.
[8] P. Nakmuenwai, F. Yamazaki, W. Liu, Automated Extraction of Inundated Areas from Multi-Temporal Dual-Polarization RADARSAT-2 Images of the 2011 Central Thailand Flood, Remote Sens. 9 (1) (2017).
[9] L. Moya, C. Geiß, M. Hashimoto, E. Mas, S. Koshimura, G. Strunz, Disaster intensity-based selection of training samples for remote sensing building damage classification, IEEE Trans. Geosci. Remote Sens. 59 (10) (2021) 8288–8304.
[10] E. Mas, D. Felsenstein, L. Moya, A.Y. Grinberger, R. Das, S. Koshimura, Dynamic integrated model for disaster management and socioeconomic analysis (DIM2sea), J. Disaster Res. 13 (7) (2018) 1257–1271, http://dx.doi.org/10.20965/jdr.2018.p1257.
[11] A. Musa, O. Watanabe, H. Matsuoka, H. Hokari, T. Inoue, Y. Murashima, Y. Ohta, R. Hino, S. Koshimura, H. Kobayashi, Real-time tsunami inundation forecast system for tsunami disaster prevention and mitigation, J. Supercomput. 74 (7) (2018) 3093–3113.
[12] G. Lämmel, D. Grether, K. Nagel, The representation and implementation of time-dependent inundation in large-scale microscopic evacuation simulations, Transp. Res. C 18 (1) (2010) 84–98, http://dx.doi.org/10.1016/j.trc.2009.04.020.
[13] E. Mas, A. Suppasri, F. Imamura, S. Koshimura, Agent-based simulation of the 2011 great east Japan earthquake/tsunami evacuation: An integrated model of tsunami inundation and evacuation, J. Natural Disaster Sci. 34 (1) (2012) 41–57, http://dx.doi.org/10.2328/jnds.34.41.
[14] M. D'Orazio, L. Spalazzi, E. Quagliarini, G. Bernardini, Agent-based model for earthquake pedestrians' evacuation in urban outdoor scenarios: Behavioural patterns definition and evacuation paths choice, Saf. Sci. 62 (2014) 450–465.
[15] K. Yamori, Revisiting the concept of tsunami tendenko: Tsunami evacuation behavior in the great east Japan earthquake, 2014, pp. 49–63, Studies on the 2011 off the pacific coast of Tohoku earthquake.
[16] C. Flores, H.S. Lee, E. Mas, J. Salar, Tsunami evacuation in a massive crowd event using agent-based model, Coastal Eng. Proc. (37) (2023) 62, http://dx.doi.org/10.9753/icce.v37.management.62.
[17] A. Suppasri, M. Kitamura, D. Alexander, S. Seto, F. Imamura, The 2024 noto peninsula earthquake: Preliminary observations and lessons to be learned, Social Sci. Res. Netw. (2024) http://dx.doi.org/10.2139/ssrn.4760347.
[18] G. Alvarez, M. Quiroz, J. León, R. Cienfuegos, Identification and classification of urban micro-vulnerabilities in tsunami evacuation routes for the city of iquique, Chile, Natural Hazards Earth Syst. Sci. Discuss. (2018) 1–20, http://dx.doi.org/10.5194/nhess-2017-458.
[19] S. El-Tantawy, B. Abdulhai, H. Abdelgawad, Multiagent reinforcement learning for integrated network of adaptive traffic signal controllers (MARLIN-ATSC): Methodology and large-scale application on downtown toronto, IEEE Trans. Intell. Transp. Syst. 14 (3) (2013) 1140–1150, http://dx.doi.org/10.1109/tits.2013.2255286.
[20] H. Lee, Human crowd evacuation framework and analysis using look-ahead-based reinforcement learning algorithm, Int. J. Dig. Human 1 (3) (2016) 248, http://dx.doi.org/10.1504/ijdh.2016.079893.
[21] Z. Yao, G. Zhang, D. Lu, H. Liu, Data-driven crowd evacuation: A reinforcement learning method, Neurocomputing 366 (2019) 314–327, http://dx.doi.org/10.1016/j.neucom.2019.08.021.
[22] Y. Xue, R. Wu, J. Liu, X. Tang, Crowd evacuation guidance based on combined action reinforcement learning, Algorithms 14 (1) (2021) 26, http://dx.doi.org/10.3390/a14010026.
[23] J. Sharma, P.-A. Andersen, O.-C. Granmo, M. Goodwin, Deep Q-learning with Q-matrix transfer learning for novel fire evacuation environment, IEEE Trans. Syst. Man Cybern. Syst. 51 (12) (2020) 7363–7381.

[24] J.A. Boyan, M.L. Littman, Packet routing in dynamically changing networks: A reinforcement learning approach, in: Proceedings of the 6th International Conference on Neural Information Processing Systems, NIPS '93, Morgan Kaufmann Publishers Inc., San Francisco, CA, USA, 1993, pp. 671–678.
[25] K. Tian, S. Jiang, Reinforcement learning for safe evacuation time of fire in Hong Kong-Zhuhai-Macau immersed tube tunnel, Syst. Sci. Control Eng. 6 (2) (2018) 45–56, http://dx.doi.org/10.1080/21642583.2018.1509746.
[26] D. Li, Z. Zhang, B. Alizadeh, Z. Zhang, N. Duffield, M.A. Meyer, C.M. Thompson, H. Gao, A.H. Behzadan, A reinforcement learning-based routing algorithm for large street networks, Int. J. Geogr. Inf. Sci. 38 (2) (2024) 183–215.
[27] S. Fraser, G.S. Leonard, H. Murakami, I. Matsuo, Tsunami vertical evacuation buildings–lessons for international preparedness following the 2011 great east Japan tsunami, J. Disaster Res. 7 (448) (2012).
[28] E. Mas, B. Adriano, S. Koshimura, An integrated simulation of tsunami hazard and human evacuation in La Punta, Peru, J. Disaster Res. 8 (2) (2013) 285–295.
[29] R.S. Sutton, A.G. Barto, Reinforcement learning: An introduction, MIT Press, 2018.
[30] T. Takabatake, T. Shibayama, M. Esteban, H. Ishii, G. Hamano, Simulated tsunami evacuation behavior of local residents and visitors in kamakura, Japan, Int. J. Disaster Risk Reduct. 23 (2017) 1–14.
[31] E.W. Dijkstra, A note on two problems in connexion with graphs, Numer. Math. 1 (1959) 269–271.
[32] Cabinet Office of Japan, Nankai trough earthquake disaster prevention measures (Japanese), 2021, available at https://www.bousai.go.jp/jishin/nankai/index.html. (Online; Last Accessed 15 May 2024).
[33] M. Hyodo, T. Hori, K. Ando, T. Baba, The possibility of deeper or shallower extent of the source area of nankai trough earthquakes based on the 1707 hoei tsunami heights along the Pacific and seto inland sea coasts, southwest Japan, Earth Planets Space 66 (2014) 1–14.
[34] K. Goda, T. Yasuda, N. Mori, A. Muhammad, R. De Risi, F. De Luca, Uncertainty quantification of tsunami inundation in kuroshio, kochi prefecture, Japan, using the nankai–tonankai megathrust rupture scenarios, Nat. Hazards Earth Syst. Sci. 20 (11) (2020) 3039–3056, http://dx.doi.org/10.5194/nhess-20-3039-2020, URL https://nhess.copernicus.org/articles/20/3039/2020/.
[35] Y. Fukushima, T. Nishikawa, Y. Kano, High probability of successive occurrence of nankai megathrust earthquakes, Sci. Rep. 13 (1) (2023) 63.
[36] A. Muhari, F. Imamura, T. Arikawa, A.R. Hakim, B. Afriyanto, Solving the puzzle of the September 2018 Palu, Indonesia, tsunami mystery: clues from the tsunami waveform and the initial field survey data, J. Disaster Res. 13 (Scientific Communication) (2018) sc20181108.
[37] M. Di Mauro, K. Megawati, V. Cedillos, B. Tucker, Tsunami risk reduction for densely populated southeast Asian cities: analysis of vehicular and pedestrian evacuation for the city of padang, Indonesia, and assessment of interventions, Natural Hazards 68 (2013) 373–404.
[38] B. Adriano, Y. Fujii, S. Koshimura, E. Mas, A. Ruiz-Angulo, M. Estrada, Tsunami source inversion using tide gauge and DART tsunami waveforms of the 2017 Mw8. 2 Mexico earthquake, Pure Appl. Geophys. 175 (2018) 35–48.
[39] J. Martínez, H. Tavera, Modelado numérico del avance de las olas del tsunami por el cauce del río Camaná, Ministerio del Ambiente, 2016.
[40] I.A. Solís, P. Gazmuri, Evaluation of the risk and the evacuation policy in the case of a tsunami in the city of iquique, Chile, Natural Hazards 88 (2017) 503–532.
[41] J. León, P.A. Catalán, A. Gubler, Assessment of top-down design of tsunami evacuation strategies based on drill and modelled data, Front. Earth Sci. 9 (2021) 744193.
[42] C. Jimenez, J. Morales, M. Estrada, B. Adriano, E. Mas, S. Koshimura, Estimation of the seismic source of the 1974 lima peru earthquake and tsunami (mw 8.1), J. Disaster Res. 18 (8) (2023) 825–834.
[43] C. Jimenez, N. Moggiano, E. Mas, B. Adriano, Y. Fujii, S. Koshimura, Tsunami waveform inversion of the 2007 Peru (Mw8. 1) earthquake, J. Disaster Res. 9 (6) (2014) 954–960.
[44] L. Otero, J. Restrepo, M. Gonzalez, Tsunami hazard assessment in the southern Colombian Pacific basin and a proposal to regenerate a previous barrier island as protection, Nat. Hazards Earth Syst. Sci. 14 (5) (2014) 1155–1168.
[45] Japan Meteorological Agency, Tsunami warning/advisory and tsunami information, 2013, https://www.data.jma.go.jp/eqev/data/en/guide/tsunamiinfo.html. (Accessed: 21 October 2024).
[46] NOAA/National Weather Service, Tsunami frequently asked questions, 2024, https://www.tsunami.gov/?page=tsunamiFAQ. (Accessed: 21 October 2024).
[47] C. Jiménez, E. Ortega, N. Moggiano, D. Olcese, P. Quispe, Tsunamis in Peru, Technical Report, Dirección de Hidrografía y Navegación, Lima, Peru, 2023, URL . (Accessed: 21 october 2024).
[48] C. Chen, M.K. Lindell, H. Wang, Tsunami preparedness and resilience in the cascadia subduction zone: A multistage model of expected evacuation decisions and mode choice, Int. J. Disaster Risk Reduct. 59 (2021) 102244.
[49] M.K. Lindell, A. Bostrom, J.D. Goltz, C.S. Prater, Evaluating hazard awareness brochures: Assessing the textual, graphical, and numerical features of tsunami evacuation products, Int. J. Disaster Risk Reduct. 61 (2021) 102361.
[50] M.K. Lindell, M.C. Jung, C.S. Prater, D.H. House, Improving cascadia subduction zone residents' tsunami preparedness: quasi-experimental evaluation of an evacuation brochure, Nat. Hazards 114 (1) (2022) 849–881.
[51] M.K. Lindell, M.C. Jung, C.S. Prater, D.H. House, US Pacific coast communities' past preparedness and preparedness intentions for cascadia subduction zone tsunamis, Int. J. Disaster Risk Reduct. 84 (2023) 103466.
[52] M.K. Lindell, M.C. Jung, C.S. Prater, D.H. House, Evaluation of hazard brochures using topic viewing durations: application to tsunami evacuation brochures, Risk Anal. 43 (10) (2023) 2129–2146.
[53] T. Takabatake, M. Esteban, I. Nistor, T. Shibayama, S. Nishizaki, Effectiveness of hard and soft tsunami countermeasures on loss of life under different population scenarios, Int. J. Disaster Risk Reduct. 45 (2020) 101491.
[54] C. Chen, C. Koll, H. Wang, M.K. Lindell, An interdisciplinary agent-based evacuation model: integrating the natural environment, built environment, and social system for community preparedness and resilience, Natural Hazards Earth Syst. Sci. Discuss. 23 (2) (2023) 733–749.
[55] C. Chen, H. Wang, M.K. Lindell, M.C. Jung, M. Siam, Tsunami preparedness and resilience: Evacuation logistics and time estimations, Transp. Res. D: Transp. Environ. 109 (2022) 103324.
[56] S.W. Tweedie, J.R. Rowland, S.J. Walsh, R.P. Rhoten, P.I. Hagle, A methodology for estimating emergency evacuation times, Soc. Sci. J. 23 (2) (1986) 189–204.
[57] M.K. Lindell, C.S. Prater, Critical behavioral assumptions in evacuation time estimate analysis for private vehicles: Examples from hurricane research and planning, J. Urban Plann. Dev. 133 (1) (2007) 18–29.
[58] M. Favereau, L.F. Robledo, D. Villalobos, P.-Y. Descote, On disasters evacuation modeling: From disruptive to slow-response decisions, Int. J. Disaster Risk Reduct. 67 (2022) 102678.
[59] M.K. Lindell, C.S. Prater, C.E. Gregg, E.J. Apatu, S.-K. Huang, H.C. Wu, Households' immediate responses to the 2009 American samoa earthquake and tsunami, Int. J. Disaster Risk Reduct. 12 (2015) 328–340.
[60] H. Wang, M.K. Lindell, M.R.K. Siam, C. Chen, R. Husein, Local residents' immediate responses to the 2018 Indonesia earthquake and tsunami, Earthq. Spectra 38 (4) (2022) 2835–2865.
[61] D.C. Han, T. Takabatake, M. Esteban, T. Shibayama, Development and implementation of a smartphone application for tsunami evacuation, Int. J. Disaster Risk Reduct. 96 (2023) 103915.